35th Annual International Conference of the IEEE EMBS
Osaka, Japan, 3 - 7 July, 2013

A Real-Time Spectral Mapper as an Emerging Diagnostic Technology in Biomedical Sciences *

George Epitropou, *Student Member, IEEE*, Vassilis Kavvadias, Dimitris Iliou, Efstathios Stathopoulos, and Costas Balas, *Member, IEEE*

Abstract— **Real time spectral imaging and mapping at video rates can have tremendous impact not only on diagnostic sciences but also on fundamental physiological problems. We report the first real-time spectral mapper based on the combination of snap-shot spectral imaging and spectral estimation algorithms. Performance evaluation revealed that six band imaging combined with the Wiener algorithm provided high estimation accuracy, with error levels lying within the experimental noise. High accuracy is accompanied with much faster, by 3 orders of magnitude, spectral mapping, as compared with scanning spectral systems. This new technology is intended to enable spectral mapping at nearly video rates in all kinds of dynamic bio-optical effects as well as in applications where the target-probe relative position is randomly and fast changing.**

I. Introduction

Spectral Imaging (SI) collects a stack of images, where each image is acquired at a narrow spectral band and all together compose the so-called spectral cube. A complete spectrum can then be calculated for every image pixel, which can be otherwise represented as a vector in a "multidimensional spectral space". In biomedical sciences there is a tremendous interest and effort towards improving and best exploiting the acquired spatio-spectral information, for obtaining diagnostic information about the compositional status of the examined tissue sample. The attractiveness of this imaging modality is that it has a great potential for becoming the basis for the development of alternative cost/effective solutions, capable of probing tissue pathologies non-invasively and at an early, curable stage (the "optical biopsy" concept) [1]. This concept has been validated in several clinical and laboratory settings (*in vivo* and *in vitro*) with various degrees of success. It should be noted however that the vast majority of biomedical applications that have been tackled with SI refer to stationary imaging conditions. This implies that current, scanning SI technologies are mostly suitable for applications where the target-probe relative position and/or the target's spectral characteristics remain unaltered throughout the entire examination time course [2]. Scanning systems record spectral images in a time-sequentially manner and calculate the spectra from *post hoc* assembly of the time-sequential data. Indicatively, typical capturing and post-capturing processing times are often in the range of several minutes, which restricts the applicability of SI to time invariant spectral features or/and to stationary target-probe imaging conditions. This can explain the limited or the cumbersome use of SI in several fields including but not limited to endoscopy, live tissue/cell imaging [3], optical molecular imaging. The ultimate solution to this high-impact problem would come from technological advancements allowing for a) the instantaneous capturing of a sufficient number of spectral images; b) the very fast, per pixel calculation of spectra and, finally, c) the display of the spectral classes' thematic map, nearly at a video rate. The ability of displaying a spectral/diagnostic map in nearly video rates is expected to substantially advance analytical sciences and change biomedical practices. The availability of the thematic map in real time will, for example, guide surgical actions, such as biopsy sampling and/or treatment, during the diagnostic scanning/interrogation of the tissue.

Several attempts have been recently reported towards achieving snapshot SI, ranging from rather trivial image replication electro optical set-ups [4] to more sophisticated methods based on coded-aperture/compressed-sensing principles, which are instantly capturing a spectral cube in the form of multiplexed spatial-spectral dimensions [5] Although these advanced approaches allow instant capturing of a multiplexed spectral cube, the associated time required for constructing a spectral thematic map is further elongated due to the computationally intensive step of decoding the captured multiplexed spectral cube. In other words current solutions are still away from delivering the complete list of targeted features (a, b, c) of the next generation of SI as set above.

In this paper we present the first 'Real Time Spectral Mapper' (RTSM) relaying on the simultaneous capturing of 6-9 real narrow band images, which comprise the experimental data for estimating the "missing" curve points and/or spectral images. Next, the calculated millions of spectra are classified and the various spectral classes, present in the scene, are displayed in the form of a color-coded spectral thematic map nearly at a video rate.

II. Material and Methods

It has been realized that accurate color reproduction is largely inaccurate when information is captured in the RGB,

* This research has been financed by the National Strategic Reference Framework (NSRF) "cooperation" action, program "OncoSeed Diagnostics: Biology of Circulating Tumour Cells, Distant Metastasis & Development of Liquid Biopsy Methods"

G. Epitropou, V. Kavvadias, D. Iliou and C. Balas are with the Department of Electronic and Computer Engineering, Technical University of Crete, Chania 73100, Crete, Greece (corresponding author to provide phone: +30-28210-37223; email: gepitropou@electronics.tuc.gr)

E. Stathopoulos is with the pathology department, Department of Medicine, University of Crete, Greece (email: stath@med.uoc.gr)

(wide) spectral bands [6]. Scanning SI technologies has been proposed as a solution to this problem [7]. However, SI instrument's and spectral cube data handling complexity, time consuming procedures, spectral image miss-registration problems etc, are suspending the adoption of this option [2]. The solution to this problem would come from new instrument designs allowing for simultaneously capturing of a sufficient number of narrow spectral bands. The generated data can be "extrapolated" to complete spectra by integrating fast and efficient spectral estimation algorithms. This set-up would provide both, metamerism-free color reproduction and fast spectroscopy.

The described RTSM was developed with the aid of our laboratory prototype scanning hyper-spectral imager (HSI), by adopting its measurements as reference spectra. This instrument performs both 3 band color and 30 band spectral imaging. The integrated efficient and fast spectral band selection mechanism is synchronized with camera sensitivity settings through computer control. Camera sensitivity settings have been determined during a calibration procedure, utilizing a white calibration sample. Calibrated imaging ensures device and ambient light independent color and spectral imaging. The HSI was used for capturing both color images and complete spectral cubes of the Macbeth ColorChecker® color patches. The fact that both color and spectral data are collected with the same, calibrated device makes the corresponding spectral prediction performances directly comparable with each other. This is untenable with other published set-ups using different instruments for performing color imaging, spectral imaging and/or spectroscopy. The complete spectral cube collected with HSI consist of 30 narrow band images (Full Width Half Max ≈ 10nm) in the range 400-700nm. The derived, from the spectral cube, spectra had 30 experimental points and comprised the reference spectra for assessing the spectral estimation performances.

There is a number of set ups that have been reported for enabling snapshot imaging but they are subjected to a series of limitations such as a) long post processing times, trade-offs between spatial and spectral resolution [5], image distortions [9], poor light throughput [10] etc. We attempted to overcome these drawbacks by developing an imaging head composed of two identical color sensors (Sony ICX204AK CCD, 1/3", 4.65 μm) and a polychroic mirror (PM) that splits the light collected by the lens onto the surfaces of the two CCD sensors. The PM transmits about 95% of the incoming light in three bands: 410-470 nm, 500-550nm 580-640nm and reflects 96% of their "complementary" bands: 470-500nm 550-580 and 640-720. Each sensor records the collected by the lens light after it has been filtered by both the sensor's RGB primary filters and the PM. With this design six spectral images can be acquired. However, the concept can be easily expanded to nine or to twelve bands by e.g. adopting image spiting optics used in e-chip color cameras. It is important to stress here that there is a substantial overlapping between the RGB primary filters transmission characteristics. Due to this fact, a given PM band is transmitted by more than one of the primary filters and at different amounts. For example, the band 410-470nm has a dominant wavelength at 430 nm and it is transmitted by the blue primary filter and finally recorded by the underlying pixel. However the tail of the Green primary filter goes down to 410 nm and due to this fact the corresponding pixel captures a fraction of the PM's 410-470nm blue band together with the PM's 550-580nm green band. It is therefore essential to disentangle the recorded spectral information for recovering the six spectral images, whose spectral content corresponds to the six transmission/reflection bands of the PM. The response R of a sensor's pixel corresponding to the ik_{th} PM's band can be modeled as follows:

$$R_{ik}(x,y) = \int_{400}^{700} PM_k(\lambda) SP_i(\lambda) E(\lambda) r(x,y;\lambda) d\lambda + n(x,y) \quad (1)$$

where PM_k is the transmittance of the k_{th} band of the PM (k=1,..6)

- $SP_i(\lambda)$ is the spectral sensitivity of the i_{th} channel (i=1..3),
- $E(\lambda)$ is the irradiance spectrum of the light source,
- $r(x,y;\lambda)$ is the reflectance spectrum of the object,
- $n(x,y)$ is the noise of the system.

In each particular camera we have measured the $SP_i(\lambda)$ of the RBG filtered cameras without the PM with the aid of grating slit monochromator. The relative spectral sensitivity $SP_i(\lambda)$ was measured across the entire 400-700nm wavelength range, from captured images of a white sample. The white sample was illuminated with the narrow band light exiting the monochromator's slit. The illuminating central wavelength was tuned and in each 3nm tuning step a color image was captured. The light power exiting the slit was maintained constant across its entire wavelength tuning range, using as feedback the measurements of a photometer (Thor Labs PM100D). By doing so, the irradiance $E(\lambda)$ was maintained constant. Moreover, the white sample has a unity reflectance $r(x,y;\lambda)$ and we can ignore the noise, as a first approximation. Under these circumstances the $SP_i(\lambda)$ can be obtained by simply measuring the $R_i(x,y)$ in all tuning steps of the monochromator, in the spectral range 400-700nm. The term $PM_k(\lambda)E(\lambda)r(x,y;\lambda)d\lambda$ of equation (1) corresponds to the transmitted by the PM k_{th} narrow band (NB_k), which reaches the i_{th} broadband filter corresponding to the i_{th} channel of the sensor. We can therefore write the response of the i_{th} channel of a given sensor to the incident light NB_k consisted of λ_k k=1,…,6 bands as follows:

$$R_i = \sum_k SP_i(\lambda_\kappa) NB(\lambda_\kappa) \quad (2)$$

With the current configuration we have six responses and provided that the $SP_i(\lambda)$ has been measured for all three channels and for all wavelengths, as described above, we can calculate the six narrow bands with spectral content defined solely for the transmittance/reflectance bands of the PM. In fact we can convert this set of equations to vector matrix notations as follows:

$$R_{ik} = SP_i NB_k \ \ or \ \ NB_k = SP_i^{-1} R_{ik} \quad (3)$$

As it can be seen the calculation of the NB_k can be straight forward, consuming insignificant computation power. The next step towards developing the RTSM was to identify the fastest and most efficient spectral estimation algorithm that

best performs with the six NB data set. The obtained results are reported below together with the performance of the conventional RGB-based spectral estimation platforms.

III. Results and Discussion

The predicted spectra were compared with the reference spectra collected with the HSI system using the Spectral Angle Mapper (SAM) [2] as a spectral similarity metric. To this end, a long list of spectral prediction algorithms such as Wiener, fast Fourier transform, principal component analysis, wavelets, singular value decomposition (SVD), and discrete cosine transform (DCT) [6],[8] were comparatively evaluated. It was found that the estimation accuracy of Wiener and fast Fourier transform algorithms were clearly superior over the other algorithms. At the same time the execution speed of these, high-ranked algorithms, was found to be higher, by at least one order of magnitude as compared with the lower ranked ones. Wiener algorithm was found to be slightly faster than FFT and for this reason it was finally chosen and integrated to the RTSM for performing the spectral estimation task. Table I shows the results (mean value ± standard deviation) of the spectral estimation accuracy in (SAM) radian units. From the physical perspective, the lower the SAM values, the higher the spectral similarity between reference and estimated spectra.

The first two cells of the table refer to Wiener estimation. The first cell has as input the three RGB broad-bands (3BB) obtained with the HSI, operating in the color imaging mode. The displayed SAM values express the similarity degree between the 3BB/Wiener-predicted spectra with the experimental spectra collected with the HSI system. The second cell's value is the result of the comparison of the RTSM's 6NB/Wiener combination-predicted spectra with the HSI experimental spectra. The third cell refers to the comparison with HSI's experimental data of a spectral line generated by simply fitting (using cubic splines) the six experimental points, generated by the RTSM. In all cases, experimental and estimated data refer to the complete panel of the Macbeth ColorChecker® patches. From each color patch, 20 reference spectra were collected with HSI. As it can be clearly seen, there is a great statistical difference (CI 95%) between the performances of the tested set-ups. The RTSM (6NB/Wiener) demonstrated superior performance than HSI (3BB/Wiener) by 45.7%. When comparing the performance of RTSM (6NB/Wiener) with the performance of the fitted 6NB, the improvement becomes much greater, reaching the value of 115%. Notably, the 3BB/Wiener demonstrates superior performance by 16.1% when it is compared with the fitted 6NB. These results suggest that increasing the number of bands is not the key alone for converging to the true values of the spectrum. It needs to be combined with efficient spectral estimation algorithms.

Table 1 Spectral Estimation Accuracy (Mean Value ± Standard Deviation)

Wiener Spectral Estimation		Cub. Spline Fitting
3BB (HSI_RGB), (MV ± SD) rad	6NB (RTSM) (MV ± SD) rad	6NB (RTSM) (MV ± SD) rad
0,1061 ± 0,0252	0,0576 ± 0,0180	0,1239 ± 0,0292

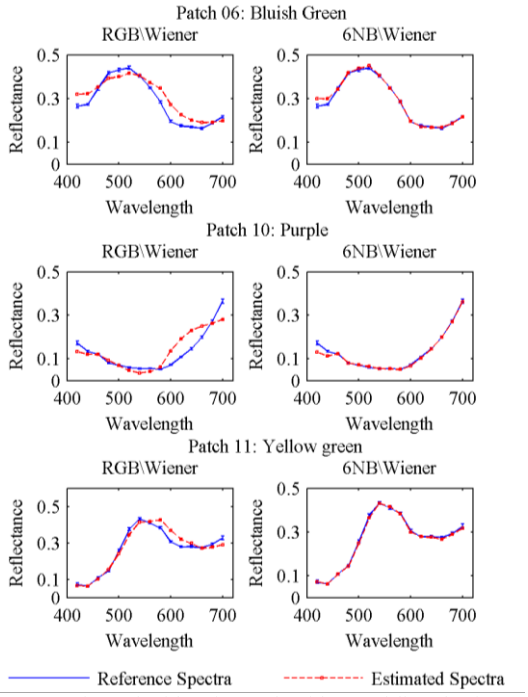

Fig 1: Spectra estimated with Wiener algorithm (red line) having as input RGB values of a color camera (left) and the six narrow bands of the RTSM (right). Blue lines are reference spectra collected with a scanning hyperspectral imager.

Fig.1 illustrates the reference and the estimated spectra obtained with the 3BB/Wiener and the 6NB/Wiener set-ups, from 3 color patches of the Macbeth ColorChecker®. The miss-fitting of the experimental data is obvious when the 3BB is used as input. On the contrary the RTSM achieves exceptional performance, with the miss-fitting lying below the experimental error associated with the collection of the reference spectra (aprox. 3% in 15000 spectra collected with HIS from each patch).

As a second-level evaluation, the RTSM was used for performing real-time feature extraction from immunostained invasive histology breast cancer samples. The purpose of the analysis was to validate its accuracy when a natural target is analyzed. The invasive ductal breast carcinoma biopsy samples were immunostained for estrogen receptors (ERs) [utilizing the Quanto UltraVision HRP Immunodetection Kit (Thermo Scie., USA) and a primary antihuman Rabbit Monoclonal antibody (SP1 RM-9101, Neomarkers, USA, with DAB as chromogen)], and counterstained with Hematoxylin. Spectral mapping was performed with both the scanning HSI system and the RTSM, both adapted to a microscope (Olympus BX51). Fig.2a, b illustrate the experimental transmittance spectra of DAB (a) and hematoxylin (b) (blue line), together the corresponding 6NB/Wiener estimated spectra (read lines). As it can be seen the experimental data are very well approximated with the predicted spectra. Fig. 2 c and d illustrate spectral maps obtained with HSI and RTSM correspondingly, overlaid onto the original color image of the sample (d). In these color-coded images, pseudocolors represent different spectral classes and depict different immunostain uptake levels from the cell nuclei, which is of great diagnostic

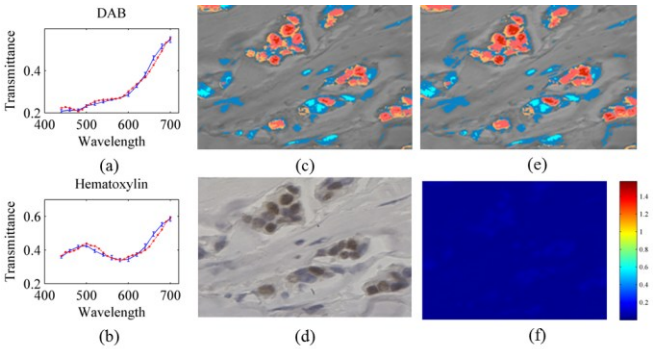

Figure 2. The experimental transmittance spectra of DAB (a) and hematoxylin (b) (blue line), together the corresponding 6NB/Wiener estimated spectra (red lines). Spectral class maps obtained with hyperspectral imaging (c) (with all data being experimental) and with six band snap-shot imaging combined with the Wiener sprectal estimation algorithm (e). Spectral mapping was performed in histologically immunostained (for estrogen receptors) invasive breast cancer biopsy sample (d). The differences between the experimental and experimental/predicted spectra are mapped in (f). The differences were measured with the spectral angle mapper and found to be less than 0,5 radians.

importance[11]. Fig. 2(f) illustrates an image depicting quantitatively the differences between the experimental spectral cube collected with the HSI system and the spectral cube generated by the RTSM. Both cubes were obtained from the histology sample of fig. 2 (d). The comparison (in radians) was performed on a pixel-by-pixel level, using (again) the SAM algorithm for comparing spectra corresponding to the same spatial coordinates. The maximum spectral difference that was measured accross the image was 0.5 radians, indicating an exceptional similarity between the measured and the estimated spectral cube. When the scanning HSI system was used, it required 100 s for completing all the tasks up to calculating the spectral map (fig. 2c). For completing the same task (fig. 2e) the RTSM system consumed just 100 ms. The spatial resolution was common (1280x960) in both systems. This makes RTSM three orders of magnitude faster than conventional scanning technologies. It is worth noticing here that this performance enables, for the first time, spectral classes to be displayed nearly at video rates and at full (high) resolution in a consumer class pc (Intel i7 2.0 GHz, 6 GB Ram) and without using additional data procesing hardware (DSPs or FPGAs). We are quite confident that by simply adding the later to the RTSM platform, speeds will by far exceed video rates. Another important advantage of the described RTSM is its very high light throughtput of about 95%, being also polarization independent. This is very essential in a variety of biomedical fields where a low excitation light energy needs to be used for avoiding damaging of the sample or for preventing photobleaching effects in flouorophores. On top of it, high light throughput relaxes the requirements for long sensor exposure times, which would result in slowing down the frame rate. Low light-throughput and polarization dependency are the most common limitations of fast scanning spectral images based on acoustooptic or liquid crystal tunable filters [2]. These devices offer ms or μs level tuning speeds but they suffer from low and non-uniform throughput, ranging from 5% to 45%. Due to their low throughput, the sensor operates at long exposure times (1-10s or more), which results to their high tuning speed remaining practically unexploitable. This is because the speed at which the spectral cube is collected is mainly determined by the (long) sensor's exposure time in each tuning step and not by the filter's tuning step. Even in that stationary-target application, it is expected, upon adoption, to increase significantly the pathology department's workfllow, while at the same time improve its objectiveness and accuracy. We are currently working on developing its application to endoscopy and to molecular imaging setups and the results obtained so far are very encouraging.

IV. Conclusions

We report the first real time spectral mapper combining snapshot spectral imaging with the Wiener spectral estimation algorithm. The descriced RTSM system offers accurate spectral mapping as compared to scanning spectral imager, being, however, three orders of magnitude faster than conventional technologies. The technology is intended to enable spectral imaging and mapping in a series of biomedical in vivo and in vitro applications involving dynamic bio-optical phenomena and not stationary imaging conditions.

References

[1] C. Balas "Review of biomedical optical imaging—a powerful, non-invasive, non-ionizing technology for improving in vivo diagnosis," Meas. Sci. Technol. IoP, vol. 20, no. 10, 2009

[2] C. Balas, G. Epitropou and C. Pappas: "Multi/Hyper-Spectral Imaging," *in Handbook of Biomedical Optics*, Taylor&Francis Books, Inc, USA, 2011

[3] Balas, C.; , "A novel optical imaging method for the early detection, quantitative grading, and mapping of cancerous and precancerous lesions of cervix, " *Biomedical Engineering, IEEE Transactions on* , vol.48, no.1, pp.96-104, Jan. 2001

[4] S. H. Hardarson, et al, "Automatic Retinal Oximetry," *Investigative Ophthalmology & Visual Science,* vol. 47, no. 11, pp. 5011–5016, Nov. 2006.

[5] A. a. Wagadarikar, R. John, R. Willett, and D. J. Brady, "Single disperser design for compressive, single-snapshot spectral imaging," *Proc. SPIE 6714, Adaptive Coded Aperture Imaging and Non-Imaging Sensors,* p. 67140A, 2007.

[6] P. Stigell, K. Miyata, and M. Hauta-Kasari, "Wiener estimation method in estimating of spectral reflectance from RGB images," *Pattern Recognition and Image Analysis*, vol. 17, no. 2, pp. 233–242, Jun. 2007.

[7] H. Haneishi, et al, "System Design for Accurately Estimating the Spectral Reflectance of Art Paintings," *Appl. Opt.*, vol. 39, no. 35, pp. 6621–6632, Dec. 2000.

[8] A. Mansouri, T. Sliwa, J. Y. Hardeberg, and Y. Voisin, "Representation and estimation of spectral reflectances using projection on PCA and wavelet bases," *Color Research & Application*, vol. 33, no. 6, pp. 485–493, Dec. 2008.

[9] W. R. Johnson, D. W. Wilson, W. Fink, M. Humayun, and G. Bearman, "Snapshot hyperspectral imaging in ophthalmology," *Journal of Biomedical Optics*, vol. 12, no. 1, p. 14036, Jan. 2007.

[10] I. T. O. Mami et al, "Oxygen saturation levels in the juxta-papillary retina in eyes with glaucoma," *Experimental eye research*, vol. 86, no. 3, pp. 512–518, 2008.

[11] Papadakis, A., *et al*. "A novel spectral microscope system: application in quantitative pathology," *Biomedical Engineering, IEEE Transactions* on, vol. 50, no. 2, 207-217, Feb. 2003